Dynamical and structural properties of a granular model for a magnetorheological fluid

F. Donado and J. M. Sausedo-Solorio
Instituto de Ciencias Básicas e Ingeniería, Universidad Autónoma del Estado de Hidalgo, Pachuca 42184, Hidalgo, México

R. E. Moctezuma*
CONACYT-Instituto de Física "Manuel Sandoval Vallarta", Universidad Autónoma de San Luis Potosí, Alvaro Obregón 64, 78000 San Luis Potosí, S.L.P., México

(Received 23 November 2016; revised manuscript received 16 January 2017; published 3 February 2017)

We study a two-dimensional nonvibrating granular system as a model of a magnetorheological fluid. The system is composed of magnetic steel particles on a horizontal plane under a vertical sinusoidal magnetic field and a horizontal static magnetic field. When the amplitude of the horizontal field is zero, we find that the motion of the particles has characteristics similar to those of Brownian particles. A slowing down of the dynamics is observed as the particle concentration increases or the magnitude of the vertical magnetic field decreases. When the amplitude of the horizontal field is nonzero, the particles interact through effective dipolar interactions. Above a threshold in the amplitude of the horizontal field, particles form chains that become longer and more stable as time increases. For some conditions, at short time intervals, the average chain length as a function of time exhibits scaling behavior. The chain length distribution at a given time is a decreasing exponential function. The behavior of this granular system is consistent with theoretical and experimental results for magnetorheological fluids.

DOI: 10.1103/PhysRevE.95.022601

I. INTRODUCTION

Magnetorheological (MR) fluids have interesting properties that have attracted attention in both applied and basic research fields. They have many potential applications in systems where controlled energy dissipation is required [1,2]. These systems exhibit notable changes in mechanical properties such as the viscosity, yield stress, and elastic modulus when a magnetic field is applied [3]. In the absence of magnetic fields, micron-size particles in an MR fluid move randomly owing to collisions with the molecules of the liquid. In this Brownian motion, temporal correlations fall very rapidly over time. When a magnetic field is turned on, the particles acquire dipolar magnetic moments that, on average, are aligned in the magnetic field direction. Owing to the anisotropy of the dipolar interaction, the interaction between two particles can be attractive or repulsive depending on their relative positions [4]. After the magnetic field reaches a threshold, the magnetic interactions overcome the thermal interactions among particles, and an aggregation process begins. At the beginning of the process, the chains are usually one particle in thickness. As dipolar interactions continue, the chains start aggregating laterally, forming columns through a zippering mechanism [4–6]. Two chains aggregate laterally depending on whether they are in-registry or off-registry [4]. Moreover, the Brownian motion causes mechanical deformation in the chains, which leads to an anisotropy of the magnetic field, enhancing and hastening this lateral aggregation. Particle size dispersion also contributes to lateral aggregation.

The kinetic theory states that at short time intervals, Brownian particles follow ballistic behavior that becomes diffusive after collisions with other particles occur [7]. In the ballistic regime, the temporal dependence of the mean squared displacement reveals quadratic behavior, whereas in the diffusive regime, the behavior is linear. In an MR fluid, when a magnetic field is applied, the transition from diffusive behavior to an arrested state occurs so quickly that it cannot be observed in detail at short time intervals. To observe the behavior at short time scales in detail, it is necessary to observe the particle trajectories with a time resolution on the order of nanoseconds and a spatial resolution on the order of molecular sizes. Thus, detailed study of the transition from ballistic to diffusive behavior of an ensemble of magnetic Brownian particles has been out of reach using current technology. However, some progress has been made in that direction; for instance, Refs. [8–10] report that by using an optical interferometric technique, the full transition from ballistic to diffusive motion of a single confined Brownian particle was observed in detail.

The slowing down of the dynamics in MR fluids as the magnetic field increases shares some characteristics with the slowing down of the dynamics observed in a glass-forming liquid when the temperature decreases [11]. To study the slowing down of a glass-forming liquid with decreasing temperature, colloidal and granular systems have been used [12–18]. Some of the advantages of these macroscopic models are that the particles can be easily tracked in more detail than particles in molecular systems and that the interparticle interactions can be modulated by active controls [18,19].

In this study, we model the phenomena occurring in MR fluids on the basis of a nonvibrating granular system under the effect of two magnetic fields: a vertical sinusoidal field and a horizontal static magnetic field. In our two-dimensional (2D) system, particle motions are effectively restricted to the horizontal plane in which the particles lie. Thus, it differs from vertically vibrated granular systems, where particles leave the plane as they move, resulting in an effective dimension greater than two dimensions [17]. In our system, we can track the particles for a long time period, provided they remain within the field of view. We found that in the absence of the horizontal magnetic field, the particles exhibit quasiballistic behavior on short time scales, whereas at long time scales, diffusive

*rosario@ifisica.uaslp.mx

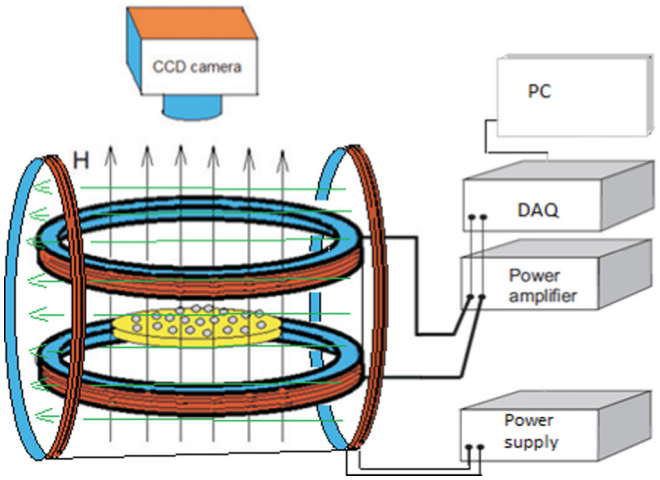

FIG. 1. Schematic diagram of the experimental setup. The vertical magnetic field is sinusoidal and the horizontal field is static.

behavior appears. This indicates that our system is suitable for modeling Brownian motion. Moreover, we found that our system is suitable for studying the role of thermal fluctuations in general, because the sinusoidal magnetic field, a parameter that plays the role of the temperature, is easily controlled by changing the intensity of the field. One example of the use of a macroscopic system to model a magnetic colloidal system can be found in Ref. [20]. There, it is reported that a system based on non-Brownian magnetic particles dispersed in a liquid, under mechanical perturbations, is suitable for studying the structures formed in a magnetic colloid [21].

In Sec. II, we describe the experimental setup. In Sec. III, we examine the slowing down of the dynamics as a function of both the particle concentration and the intensity of the vertical magnetic field. In Sec. IV, we analyze the dynamical and structural properties of the chainlike structures that are formed when a horizontal field is applied; we determine the growth rate and the distribution of chain lengths. Finally, in Sec. V, we provide our final comments and remarks.

II. EXPERIMENTAL SETUP

We conduct our experiments using a modified version of the experimental setup used in Ref. [18]. We use up to 3000 steel beads (1-mm diameter) confined in a circular plate 72 mm in diameter. The particles are homogeneous in shape and size to avoid the effects of size polydispersity. Figure 1 schematically illustrates the experimental setup. The system is located horizontally between two pairs of Helmholtz coils that produce a vertical oscillating field ($B_{\rm osc}$) and a horizontal static field ($B_{\rm static}$). The coils that produce $B_{\rm osc}$ are fed by a Kepco power amplifier driven by a sinusoidal signal. This signal is sent to the amplifier from a PC through a DAQ NI data acquisition card. The frequency of the signal is 9.25 Hz. The coils that produce $B_{\rm static}$ are fed by a PASCO power supply.

The experiments are recorded using a CCD videocamera at 30 fps in AVI interlaced format. The observation field is smaller than the confining boundaries of the sample to avoid edge effects. From the videos, we obtain 20 000 frames. During the decompression process, we use a filter to separate the even and odd frames; thus, we obtain 60-fps resolution. We obtain the trajectories of the particles by using IMAGEJ and its plugin MOSAIC [22,23]. These trajectories are used to obtain the mean squared displacement $\langle \Delta \boldsymbol{r}^2(t)\rangle$ and the intermediate scattering function $F_s(k,t)$ using programs we designed. We used stacks of frames to calculate the radial distribution function $g(r)$ and the effective potential $U_E(r)$. We study these quantities under several particle concentrations, vertical magnetic fields, and horizontal magnetic fields.

III. STRUCTURE AND DYNAMICS AS A FUNCTION OF PARTICLE CONCENTRATION AND MAGNITUDE OF THE VERTICAL MAGNETIC FIELD

We characterize the structure and dynamics of the system for various particle concentrations and amplitudes of the vertical field while keeping the horizontal field $B_{\rm static}$ at zero. Here, the particle concentration is defined as $\phi_s = \frac{N\pi d^2}{4A}$, where d is the diameter of the beads, and N is the number of particles in an area A. First, we vary the particle concentration in the range $0.013 < \phi_s < 0.545$, keeping $B_{\rm osc} = 46.7$ G. Figure 2 shows some typical trajectories observed in our system for different particle concentrations. These trajectories are similar to those observed in an ensemble of Brownian particles. At low particle concentrations, the particles enter and leave the observation window quickly, colliding a few times with other particles [Fig. 2(a)]. As the particle concentration increases, collisions are more frequent, and the particles spend more time within the field of view [Fig. 2(b)]. Furthermore, at higher concentrations, a greater slowing down of the dynamics is observed, and the particles are trapped in small cages [Fig. 2(c)].

We calculate $\langle \Delta \boldsymbol{r}^2(t)\rangle$ and $g(r)$ for several particle concentrations. In Fig. 3, we plot $\langle \Delta \boldsymbol{r}^2(t)\rangle$ for some of the particle concentrations studied here. At low particle concentrations and short time intervals, a relation of the form $\langle \Delta \boldsymbol{r}^2(t)\rangle \sim t^{1.8}$ can be fitted to the curves (not shown in the figure); thus, in this regime, the motion is quasiballistic. This regime is not studied here. At longer time intervals, the behavior changes, and it takes the form $\langle \Delta \boldsymbol{r}^2(t)\rangle \sim t$, showing diffusive behavior. As particle concentration increases, the slope of the curves becomes smaller, and the ballistic regime vanishes. Further increases in the particle concentration produce qualitative changes in $\langle \Delta \boldsymbol{r}^2(t)\rangle$ as the particles pass from diffusive to subdiffusive and then to confined behavior.

We fit a linear function to each curve of the mean squared displacement. From the slope of each curve, and using the Einstein relation $\langle \Delta \boldsymbol{r}^2(t)\rangle = 4Dt$, we determine the diffusivity D. Because some of the $\langle \Delta \boldsymbol{r}^2(t)\rangle$ curves show considerable curvature, the diffusivity we report is in fact a mean value. For low particle concentrations, the diffusivity is large, and the particles leave the field of observation very quickly. Thus, in these cases we cannot follow single particles for long times. The reentrant trajectories are taken as new trajectories. Here, after 1.66 s, large fluctuations appear in $\langle \Delta \boldsymbol{r}^2(t)\rangle$ owing to the lack of statistics because, at this point, the long trajectories are few. In the intermediate particle concentration regime, the dynamics is subdiffusive. In this regime, we can follow the trajectories for longer times. At high particle concentrations, arrested trajectories dominate the dynamics. Figure 4 shows the D value for each concentration studied here. We can observe that

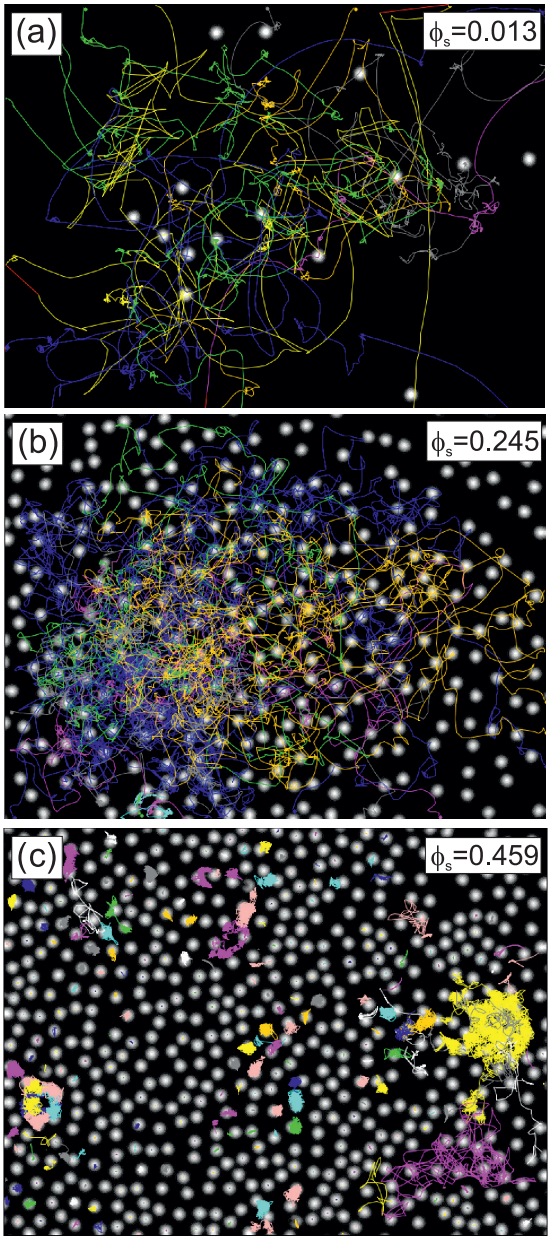

FIG. 2. Typical trajectories. (a) At low concentrations, the particles quickly leave the observation field. (b) At higher concentrations, the trajectories are larger and more intricate. The particles stay longer within the field of observation, sweeping a larger region than at low concentrations. (c) At high concentrations, only a few particles are still diffusing, and the effect of "caging" appears, trapping the particles in arrested states. The magnetic field in all three cases is $B_{\rm osc} = 46.7$ G.

D decreases very quickly, going to zero around $\phi_s = 0.52$. This indicates that at this point, the system becomes arrested.

Figure 5 shows $g(r)$ for several particle concentrations. We observe that at low concentrations, a depletion zone appears in the range $1 < r/d < 2$ [Fig. 5(a)]. The reason is that, at very low concentrations, the particles are free to move to almost any position and avoid being in close proximity to each other because of repulsive interactions. These repulsive interactions arise because, on average, the dipolar moments of the particles

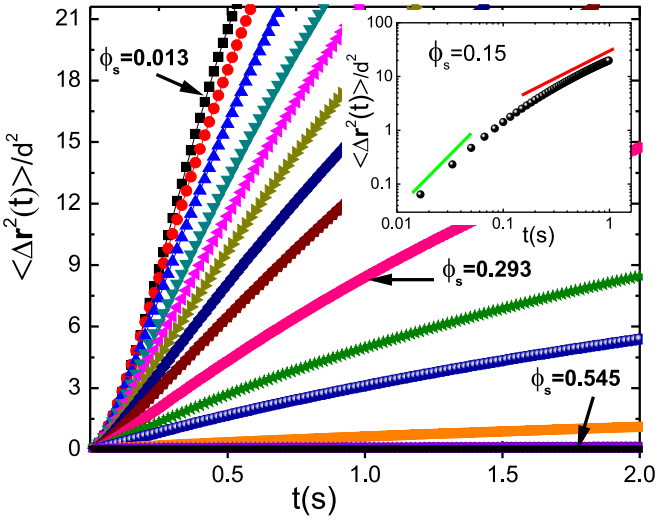

FIG. 3. Mean squared displacement for several particle concentrations. Low particle concentrations show quasiballistic (at short time scales) and diffusive (at long time scales) behavior. At high particle concentrations, the particles became arrested. The magnetic field is $B_{\rm osc} = 46.7$ G. (Inset) Mean squared displacement for a concentration of $\phi_s = 0.15$; the green and red lines have slopes of 2 (ballistic) and 1 (diffusive), respectively.

are parallel. For concentrations greater than $\phi_s = 0.076$, a small peak around $r/d = 1.25$ and a hump around $r/d = 1.75$ can be observed. The former appears because the number of collisions increases with the concentration, so the probability of finding a particle at a distance of around $r/d = 1$ increases despite the repulsive interactions. Moreover, as the particle concentration increases, some particles aggregate, and the peak is shifted toward $r/d = 1$. The hump around $r/d = 1.75$ shows that, on average, particles are at a certain distance from each other. As the particle concentration increases, collisions become more frequent, and the particles change direction more often; thus, they are forced to be closer to each other, and the hump is shifted toward the left [Fig. 5(b)]. As shown in the graphs, $g(r)$ evolves toward a liquidlike configuration as

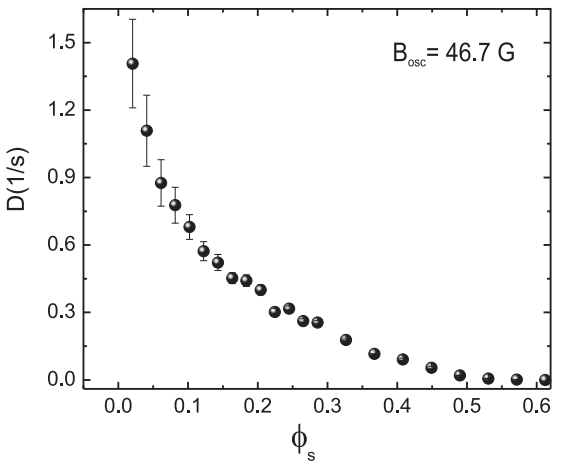

FIG. 4. Diffusivity for different particle concentrations. Note that the curve goes down very quickly as the particle concentration increases.

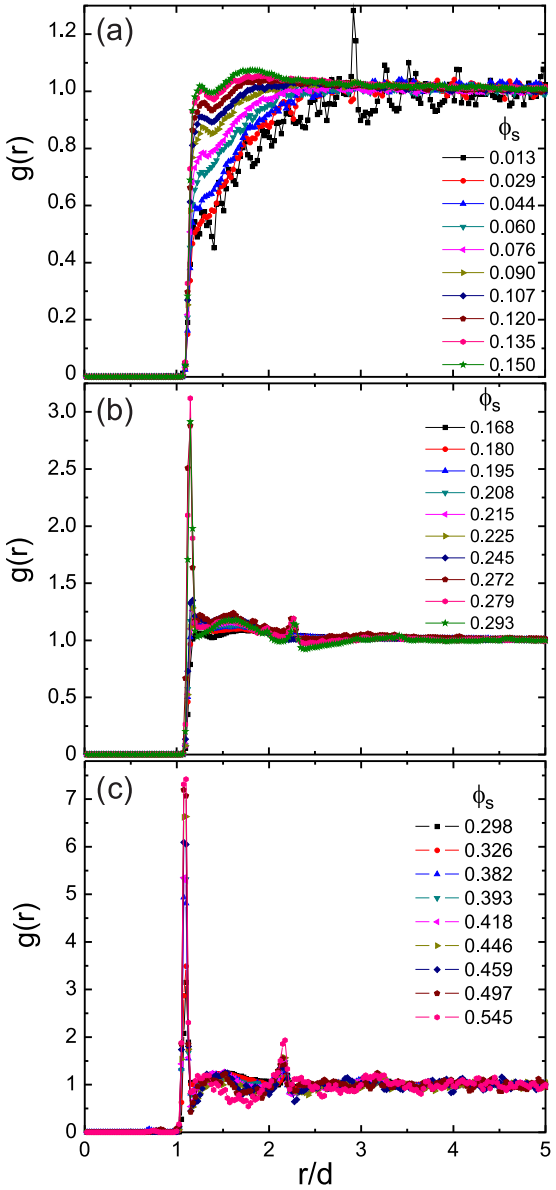

FIG. 5. Radial distribution function for different particle concentrations. (a) At low concentrations, the system exhibits a significant depletion zone in the range of 1–2 particle diameters. (b) and (c) For intermediate and high concentrations, the system starts exhibiting some features similar to those of a liquid. The magnetic field is $B_{\rm osc} = 46.7$ G.

the particle concentration increases. For the highest particle concentrations, we observe the characteristic curve for a liquid, although most of the particles in the system are arrested [Fig. 5(c)]. Thus, we have a system that evolves from gaslike behavior to solidlike behavior with a liquidlike structure, which is characteristic of the glassy state.

We determined the effective potential $U_E(r)$ to obtain information about the effective interactions among the particles in the system. We follow the method used in Ref. [18]. Briefly, it starts from the Ornstein-Zernike equation,

$$h(r_{12}) = c(r_{12}) + \phi_s \int d^3\,\mathbf{r}_3 c(r_{13}) h(r_{32}), \qquad (1)$$

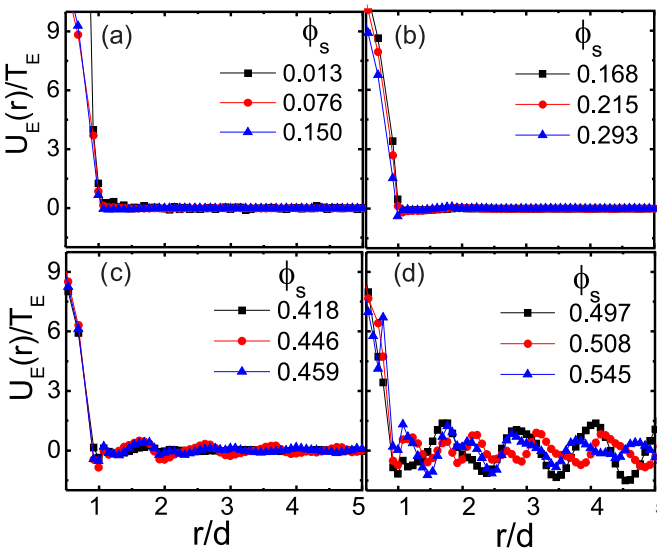

FIG. 6. Effective potential in the HNC approximation for some of the concentrations studied here.

where $h(r) = g(r) - 1$ is the total correlation function, and $c(r)$ is the direct correlation function. In the frequency space, using the fast Fourier transform (FFT), this relation is transformed to

$$\hat{c}(k) = \frac{\hat{h}(k)}{1 - \phi_s \hat{h}(k)}. \qquad (2)$$

From the experimental data, we determined $\hat{h}(k)$ using the FFT. After determining $\hat{c}(k)$, we return to real space by using the inverse FFT to obtain $c(r)$. The relationship between $c(r)$ and the effective potential $U_E(r)$ is approximately given by a closure relationship. Here, we use the hypernetted chain (HNC) approximation [7], which states that

$$h(r) - c(r) = \ln g(r) + U_E(r)/T_E, \qquad (3)$$

where T_E is the effective temperature. This relation is solved for $U_E(r)/T_E$. Here, we have followed the usual practice of setting $k_B = 1$ in granular systems [18].

In Fig. 6, we plot $U_E(r)/T_E$ in the HNC approximation for different concentrations. At low concentrations, the repulsive part of the potential governs the dynamics of the system. Here, the effective potential has a very shallow well around one-particle diameter and then becomes almost flat [Figs. 6(a) and 6(b)]. As the concentration increases, the first well becomes deeper, and other wells appear [Fig. 6(c)]. For the three highest concentrations, the effective potential exhibits periodic behavior [Fig. 6(d)].

As we stated above, the effective temperature of the system can be varied by changing $B_{\rm osc}$. In Fig. 7, we depict the behavior of the measured $\langle \Delta \boldsymbol{r}^2(t) \rangle$ for different magnitudes of $B_{\rm osc}$ with $\phi_s = 0.15$. As expected, as the temperature decreases, $\langle \Delta \boldsymbol{r}^2(t) \rangle$ decreases. Figure 8 shows the behavior of D as a function of the oscillating magnetic field ($B_{\rm osc}$). After reaching a threshold value (around 6 G), D increases linearly as

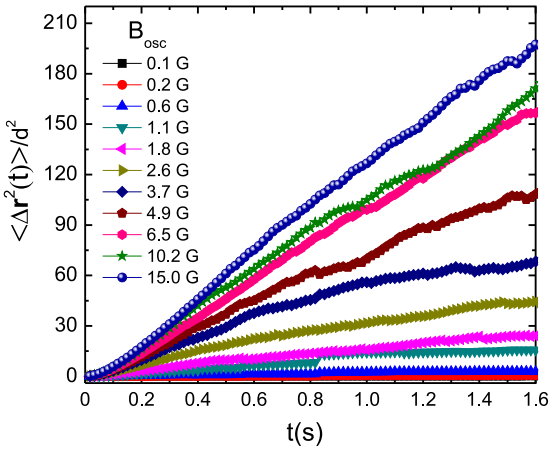

FIG. 7. Mean squared displacement for different magnitudes of the magnetic field ($B_{\rm osc}$) with $\phi_s = 0.15$. Here, we observe a transition from diffusive to arrested states.

the temperature increases. Figure 9 shows $g(r)$ and $U_E(r)/T_E$ for $\phi_s = 0.15$ and different magnitudes of the oscillating field. As $B_{\rm osc}$ decreases, we can observe an evolution similar to that observed for increasing particle concentration. As we decrease the magnitude of the field, the system evolves toward a state that exhibits a liquidlike structure [Fig. 9(a)]. The effective potential also supports this picture; it evolves toward a state with several effective attractive potential wells [Fig. 9(b)].

These results show that the dynamics and structure of the system depend on both the particle concentration and the magnitude of the oscillating field; in vibrating granular systems, the structure depends only on the particle concentration. From the above results, we select an oscillating field (effective temperature) $B_{\rm osc} = 15$ G and a particle concentration $\phi_s = 0.15$. With these parameters, the particles move diffusively. The inclusion of a horizontal magnetic field in this system under these conditions is studied in the next section.

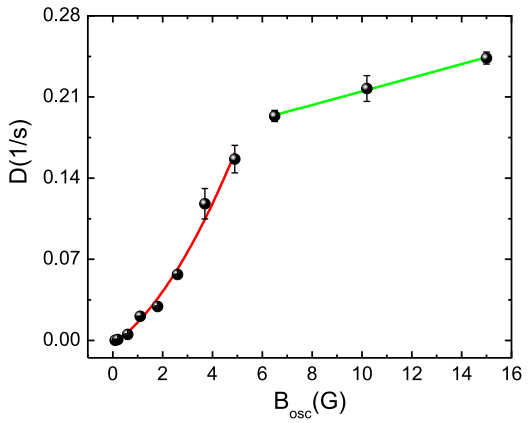

FIG. 8. Diffusivity at different magnitudes of the oscillating (vertical) magnetic field. For small field magnitudes, the diffusivity increases following a quadratic function (red continuous line) as the magnitude of the field increases. For large magnitudes, the increment is linear (green continuous line).

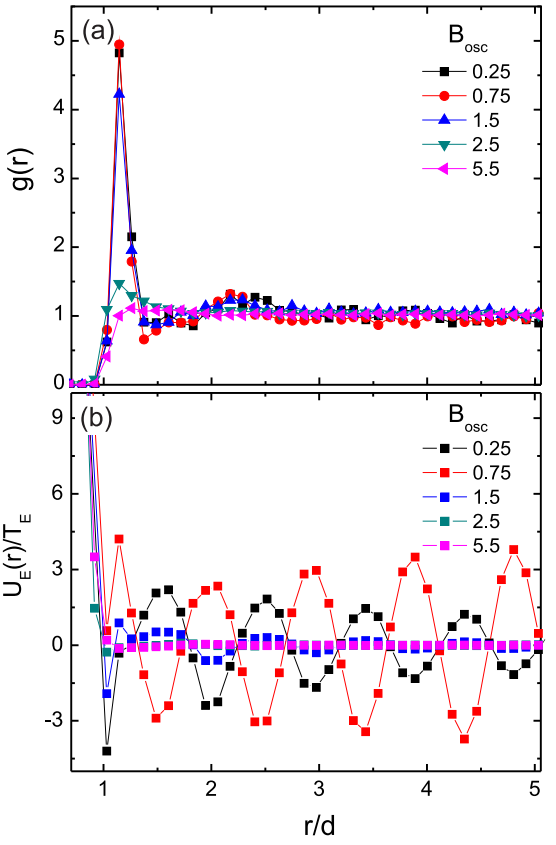

FIG. 9. (a) Radial distribution function for a fixed concentration $\phi_s = 0.15$ and different magnitudes of the vertical oscillating field $B_{\rm osc}$. (b) Effective potential in the HNC approximation for different oscillating magnetic fields.

IV. SYSTEM UNDER A HORIZONTAL MAGNETIC FIELD

To study the aggregation process due to dipolar interactions such as those studied in dipolar fluids, including MR fluids, we analyze the behavior of the system at $B_{\rm osc} = 15$ G, a concentration $\phi_s = 0.15$, and various horizontal magnetic fields. In Fig. 10, we show snapshots of the chain formation under different horizontal magnetic fields. We can observe that when the field is small (16 G), no aggregates are formed [Fig. 10(a)]. When $B_{\rm static} = 20$ G, a few aggregates that are weakly joined begin to appear [Fig. 10(b)]. For $B_{\rm static} = 23.5$ G, the aggregates increase and are more stable [Fig. 10(c)], and finally, for $B_{\rm static} = 41.5$ G, the aggregates that form are tightly bound [Fig. 10(d)].

Figure 11 shows the behavior of $\langle \Delta \boldsymbol{r}^2(t) \rangle$ as a function of the horizontal field intensity. In these curves, we observe behavior similar to that observed when the particle concentration increases (Fig. 3) or when $B_{\rm osc}$ (the temperature) decreases (Fig. 7). At low magnetic fields, the motion is diffusive and decreases as the magnetic field increases. Even though these curves show the slowing down of the particle dynamics as the magnetic field increases, this slowing down does not occur in the same way as in a glass-forming liquid as the temperature decreases. In our system, the calculated $\langle \Delta \boldsymbol{r}^2(t) \rangle$ is the average of the motion of isolated particles and the motion of particles that are forming a chain; isolated particles are very fast and move with high energy, whereas particles that are forming a

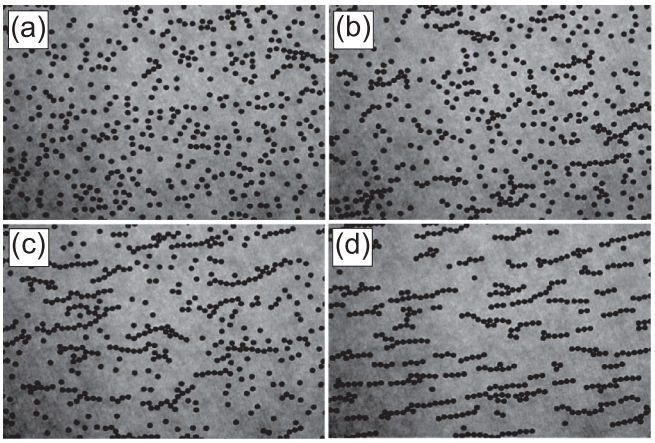

FIG. 10. Snapshots of the particle configurations for $B_{osc} = 15$ G and different horizontal magnetic fields: (a) $B_{static} = 16.0$ G, (b) $B_{static} = 20.0$ G, (c) $B_{static} = 23.5$ G, (d) $B_{static} = 41.5$ G. At small magnetic fields (a) and (b), small aggregates are formed; however, they are not very stable and are rapidly destroyed. As the magnetic field increases, the aggregates become stable (c) and (d).

chain move slowly. This behavior differs from that observed when a glass-forming liquid is cooled, where most of the particles slow down at the same rate.

Figure 12 shows the diffusivity as a function of the static magnetic field intensity (B_{static}). Here we observe that D decreases very rapidly as B_{static} increases. At low magnetic fields, small aggregates are formed; however, these aggregates are destroyed very rapidly. As the magnetic field increases, the chainlike aggregates are more stable. The inset of Fig. 12 shows D as a function of the inverse of B_{static}. In this curve, we can observe that increasing B_{static} has an effect similar to that of decreasing B_{osc} (temperature). That is why, in some studies of MR fluids, concepts from the glass transition literature are used [11].

One of these concepts is the intermediate scattering function $F_s(k,t)$ which measures the temporal correlations of the particle positions. For a homogeneous system, $F_s(k,t)$ is

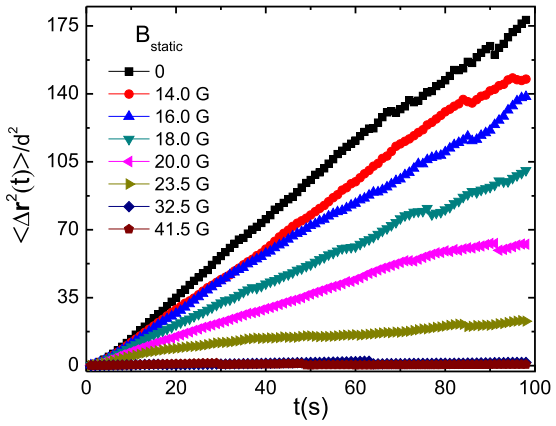

FIG. 11. Measured mean squared displacement for several horizontal magnetic fields. As the magnetic field increases, the particle dynamics changes to arrested states.

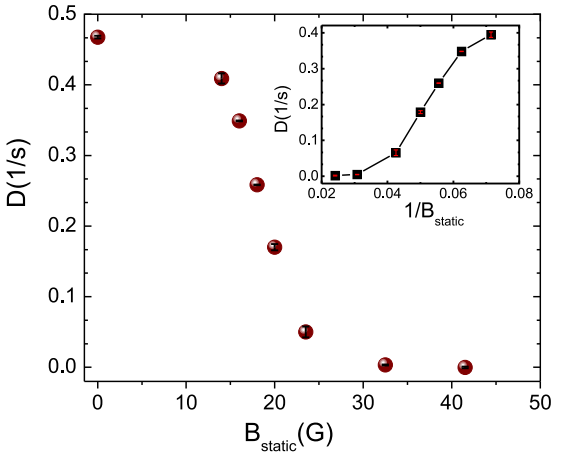

FIG. 12. Diffusivity at different magnitudes of the static (horizontal) magnetic field. The values decrease very quickly as the magnetic field increases. After reaching a value of around 40 G, the diffusivity is almost zero. (Inset) D as a function of $1/B_{static}$. Here, we can observe that increasing the horizontal field is equivalent to decreasing the oscillating field.

given by

$$F_s(k,t) = \left\langle \frac{\sin(k(r_j(t) - r_j(0)))}{k(r_j(t) - r_j(0))} \right\rangle, \tag{4}$$

where $r_j(t)$ represents the position of a particle at time t in its trajectory j. If $F_s(k,t)$ drops very quickly, it indicates that the positions are time uncorrelated; on the other hand, if $F_s(k,t)$ remains near unity, the positions are highly time correlated.

Figure 13 shows $F_s(k,t)$ curves obtained immediately after the B_{static} field is turned on. We use $k = 5$ because the first peak in $g(r)$ curves appears first at a distance of around $r/d = 1.25$; to determine k we have used $k = 2\pi/1.25$. For weak magnetic fields $F_s(k,t)$ decays very quickly, showing that the magnetic field does not produce stable structures, and consequently the

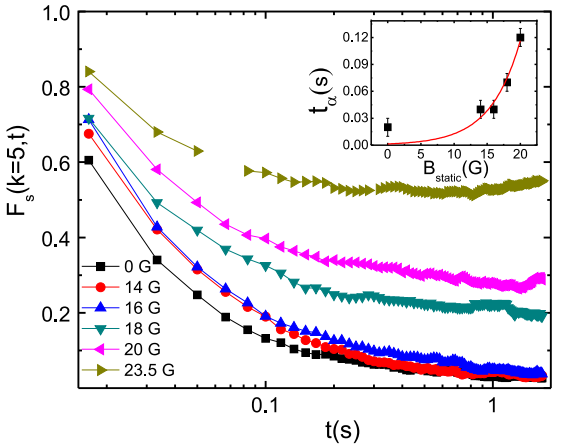

FIG. 13. Intermediate scattering function for different horizontal magnetic fields (B_{static}). As the magnetic field increases the correlation increases. For the highest magnetic field, the formation of stable structures produces high correlation curves. (Inset) α-relaxation time for different horizontal magnetic fields. The red continuous line is an exponential fitting to data.

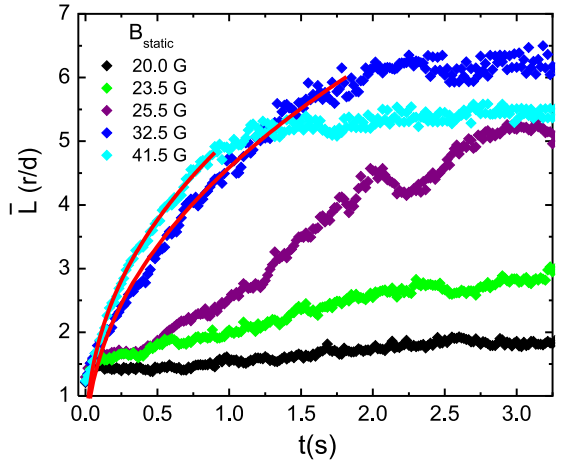

FIG. 14. Average chain length as a function of time for different magnitudes of B_{static}. At short times and large magnitudes, the curves can be fitted by a power law (red continuous lines). At small magnitudes, the behavior is more complex.

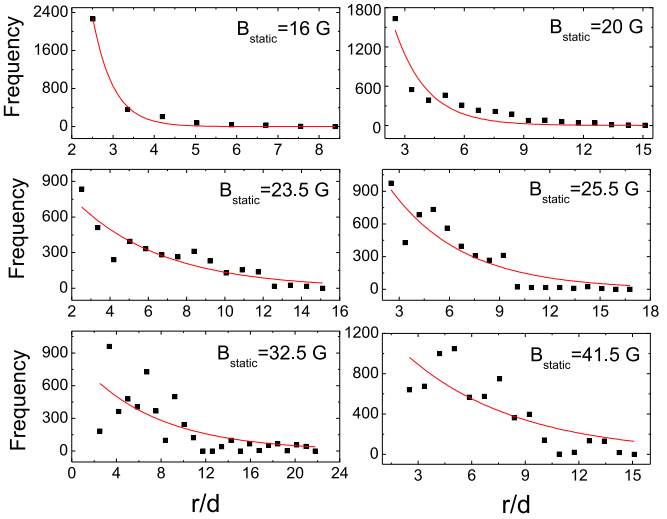

FIG. 15. Histograms of the average chain length for different static magnetic fields. Continuous lines are the exponential fittings.

temporal correlation decays very quickly. As the magnetic field increases, the $F_s(k,t)$ curves show behavior that indicates that the particle positions are correlated with the initial positions. In these cases, the time correlation indicates that stable structures are formed. The range of magnetic field intensities at which the system changes from having weak correlations to having strong correlations is very narrow. From the $F_s(k,t)$ curves, the α-relaxation time t_α is calculated by determining the time it takes for $F_s(k,t)$ to decay to $1/e$ from its initial value. As shown in the inset of Fig. 13, the α-relaxation time increases exponentially with B_{static} as in glass-forming systems as the temperature decreases.

Figure 14 shows the temporal evolution of the average chain length $\bar{L}$ for different values of the horizontal magnetic field. The chains were identified and their lengths were measured using IMAGEJ [23]. In all cases, we observe that the initial growth increases with increasing magnetic field. Furthermore, for high field intensities and short time intervals, the average chain length at time t follows power law behavior, $\bar{L} \sim t^z$. For $B_{\text{static}} = 32.5$ G and 41.5 G, we found that the kinetic exponents are $z = 0.45$ and 0.42, respectively. Similar kinetic exponents have been reported in some studies of MR fluids. For instance, in Ref. [24], the kinetic exponent in a system based on superparamagnetic particles 1μm in diameter was found to be $z = 0.57$. In a similar system, when salt was added, it was found that $z = 0.45$ [25]. On the other hand, in Ref. [26], the aggregation process of non-Brownian magnetic particles (65 μm in diameter) was studied in the presence of a static magnetic field and in the presence of two perpendicular magnetic fields (a static and an oscillating field). In that work, it was found that in the presence of only the static field, the kinetic exponent was $z = 0.3$; when both fields were applied with a low frequency of the oscillating field (1.5 Hz), the exponent was $z = 0.53$, and for a higher frequency (12 Hz), it was $z = 0.45$. Therefore, our results are in good agreement with those obtained for MR fluids. As we can see from Fig. 14, at long time intervals, the curves reach a plateau, indicating that at this point the aggregates reach their maximum length. This happens because when the horizontal magnetic field is turned on, the particles start aggregating axially, forming chains. As these chains grow, the number of isolated particles decreases until no more isolated particles remain. At this point, the chains stop growing axially. Chains cannot aggregate laterally because of friction with the container surface. In our system, there are no mechanical fluctuations in the chains such as those occurring in lateral aggregation in MR fluids [4–6,27]. Thus, the maximum growth is reached, and the plateau in the average chain length appears. On the other hand, when the field intensity is low, the growth of chains is slower, and it does not follow a power law. These results show that magnetic fields of around 30 or 40 G are needed to reproduce the formation of aggregates as in MR fluids.

We observe that, as in MR fluids, the chains that form are not all the same length but rather exhibit a distribution of lengths. Figure 15 shows the average chain length distribution for different static magnetic field intensities. Each distribution is well fitted by an exponential function of the form,

$$f((r/d)) = A_e \exp\left(-\zeta \frac{r}{d}\right), \tag{5}$$

where A_e and ζ are adjustable parameters.

In the literature on MR fluids and ferrofluids, exponential distributions have also been reported [28,29]. In Ref. [30], we theoretically and experimentally studied this distribution in an MR fluid. Here we briefly describe that result applied to our granular system. We started from an ensemble of chains of different lengths constrained to a fixed number of particles under a magnetic field. The chain length distribution can be obtained by determining the conditions that minimize the Helmholtz free energy [31–36]. In a first approximation, we can consider noninteracting chains. The proposed partition function for the ensemble is

$$Z = \prod_{n=1}^{n_{\max}} \frac{q_n^{M_n}}{M_n!}, \tag{6}$$

where q_n is the partition function of a chain with n particles, M_n is the number of chains of length n, and $n_{\max}$ is the

number of particles in the longest chains. For q_n, the sum over all its energetic states can be approximated by one term corresponding to the average configurational energy $\bar{\varepsilon}$ [7], that is,

$$q_n = \sum_i \exp\left[-\frac{\varepsilon_i}{T_E}\right] \approx \exp\left[-\frac{\bar{\varepsilon}}{T_E}\right]. \tag{7}$$

The energy $\bar{\varepsilon}$ can be approximated by the sum of the energies of pairs of particles, $-[\varphi(1,2)+\varphi(2,3)+\cdots+\varphi(n-1,n)]$. If we ignore the effects of the edges of the chains, each term could be considered equal to φ; then the partition function for a single chain is expressed as

$$q_n = \exp\left[-\frac{(n-1)\varphi}{T_E}\right]. \tag{8}$$

This expression for the partition function is in agreement with the result obtained in Ref. [31].

The distribution of chain lengths can be derived by minimizing the Helmholtz free energy,

$$F = -T_E \ln Z, \tag{9}$$

which is restricted by the conservation of particles,

$$N = \sum_{n=1}^{n_{\max}} n M_n. \tag{10}$$

Starting from the partition function in Eq. (6) and using the expression for the partition function of a single chain in Eq. (8), and minimizing the Helmholtz free energy, we find that M_n is given by

$$M_n = \exp\left(\frac{\varphi}{T_E}\right)\exp\left[-n\left(\frac{\varphi}{T_E}+\lambda\right)\right], \tag{11}$$

where λ is a Lagrange multiplier. If $n \gg 1$, it can be shown that [30]

$$N = \frac{\exp\left(\frac{\varphi}{T_E}\right)}{\left(\frac{\varphi}{T_E}+\lambda\right)^2}; \quad \bar{L} = \frac{1}{\frac{\varphi}{T_E}+\lambda}, \tag{12}$$

where $\bar{L}$ is the average chain length. In an area A of an MR fluid consisting of spherical particles of diameter d, the total number of particles N is given by

$$N = \frac{4\phi_s A}{\pi d^2}. \tag{13}$$

Therefore, using Eqs. (11)–(13), the distribution of chain lengths is given by

$$M_l = \frac{4\phi_s A}{\pi d^2 (\bar{L})^2}\exp\left(-\frac{1}{\bar{L}}\frac{r}{d}\right). \tag{14}$$

This theoretical result is in agreement with our experimental findings on MR fluids in Refs. [30,37] and with previous theoretical results [28,29,36]. This expression for the chain length distribution is also in agreement with the one we obtained in our granular model of MR fluids (Fig. 15). A more accurate expression for the chain length distribution in dipolar fluids can be found in Ref. [38]. However, that expression involves an equilibrium state with a constant concentration of isolated particles. In our case, in the conditions where chains form, the concentration of isolated particles goes to zero rapidly as chains grow.

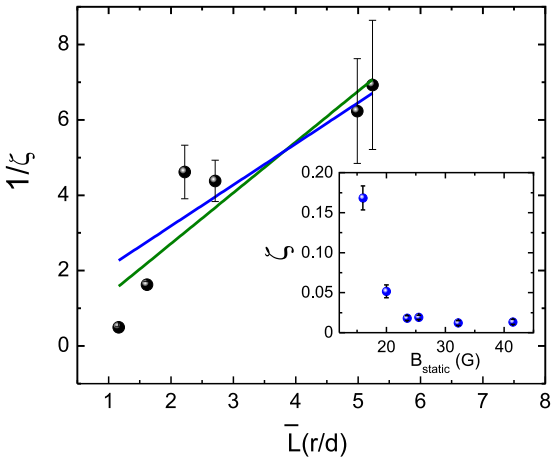

FIG. 16. Inverse of the exponential decay rate of the chain length distribution as a function of the average chain length. The green line is the linear fitting (slope of 1.3), and the blue line (slope of 1) is traced for comparison. (Inset) Exponential decay rate as a function of the static magnetic field.

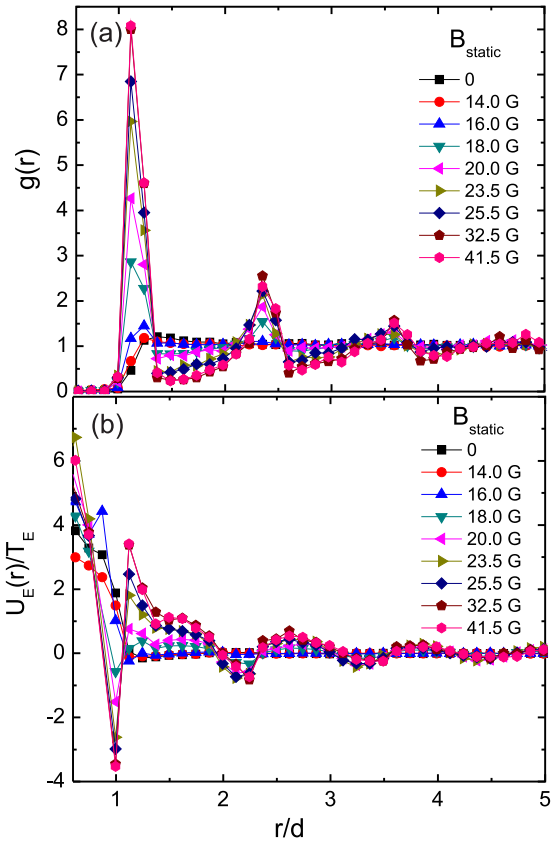

FIG. 17. (a) Radial distribution function for a fixed oscillating field $B_{\rm osc} = 15$G and several horizontal magnetic fields ($B_{\rm static}$). Note the peaks appearing around multiple particle diameters. (b) Effective potential $U_E(r)/T_E$ in the HNC approximation for different values of $B_{\rm static}$.

From Eq. (14) and Eq. (5) it can be seen that the exponential decay rate ζ and the average chain length $\overline{L}$ are inversely proportional to each other. Figure 16 compares the average chain length and the inverse of the exponential decay rate. A linear fitting shows a slope around 1.3 (green line); however, full agreement between our theory and the experimental results would require a slope of 1 (blue line). Although there is a discrepancy of around 30%, it is interesting that our granular system exhibits behavior similar to that of MR fluids.

The radial distribution function shows very sharp peaks resulting from periodic structures. In this case, these peaks correspond to chains in which particles are located in a periodic configuration [Fig. 17(a)]. Although the radial distribution function is a quantity defined for systems with radial symmetry, the curve clearly shows maxima at multiple particle diameters. Even for lower fields, the radial distribution function clearly shows signatures of these periodic arrangements (formation of straight chains). As particle concentration increases, the maxima grow in amplitude. The first peak is very notable and indicates that short chains are more numerous than longer ones.

Figure 17(b) shows the effective potential curves for different horizontal magnetic fields. The effective potential evolves from a case where repulsive interactions dominate the dynamics to a case where periodic wells are formed. The fact that the deepest well appears around one-particle diameter shows that first-neighbor interactions are more important.

V. COMMENTS AND REMARKS

We studied a nonvibrating granular system that, under a vertical sinusoidal field, exhibits behavior very similar to that of a system based on Brownian particles. The dynamical and structural characteristics of this system can be easily controlled by varying the particle concentration and the magnitude of the vertical magnetic field, which plays the role of the temperature. We applied an additional static magnetic field in the direction horizontal to the plane in which the particles lie. This second field produces an effective magnetic dipolar interaction among the particles, which in turn initiates the formation of chains of different lengths. The general process consists of the initial formation of short chains that grow with time. We found that the growth rate of the chains follows a scaling law similar to that observed in MR fluids. Our results show that this granular system can be used to model particle aggregation processes in an MR fluid under a steady magnetic field. The experimental setup can be modified to model other complex fluids since the particle concentration, the "temperature," and additional interactions can be easily controlled.

ACKNOWLEDGMENTS

Partial financial support from CONACyT-México through Soft Condensed Matter RED TEMATICA and Grant No. 256176, and from Fondo de Apoyo a la Investigación (FAI-UASLP) is acknowledged.

[1] D. J. Klingenberg, AIChE J. **47**, 246 (2001).
[2] J. Vicente, D. J. Klingenberg, and R. Hidalgo-Alvarez, Soft Matter **7**, 3701 (2011).
[3] L. J. Felicia and J. Philip, Phys. Rev. E **89**, 022310 (2014).
[4] R. E. Moctezuma, F. Donado, and J. L. Arauz-Lara, Phys. Rev. E **88**, 032305 (2013).
[5] E. M. Furst and A. P. Gast, Phys. Rev. E **62**, 6916 (2000).
[6] J. M. Laskar, J. Philip, and B. Raj, Phys. Rev. E **80**, 041401 (2009).
[7] D. A. McQuarrie, *Statistical Mechanics* (University Science Books, Herndon, 2000).
[8] P. N. Pusey, Science **332**, 802 (2011).
[9] T. Li, S. Kheifets, D. Medellin, and M. G. Raizen, Science **328**, 1673 (2010).
[10] R. Huang, I. Chavez, K. M. Taute, B. Lukić, S. Jeney, M. G. Raizen, and E.-L. Florin, Nat. Phys. **7**, 576 (2011).
[11] J. Vicente and C. L. A. Berli, Rheol. Acta **52**, 467 (2013).
[12] G. L. Hunter and E. R. Weeks, Rep. Prog. Phys. **75**, 066501 (2012).
[13] E. R. Weeks, J. C. Crocker, A. C. Levitt, A. Schofield, and D. A. Weitz, Science **287**, 627 (2000).
[14] H. König, K. Zahn, and G. Maret, AIP Conf. Proc. **708**, 40 (2004).
[15] H. König, Europhys. Lett. **71**, 838 (2005).
[16] H. König, R. Hund, K. Zahn, and G. Maret, Eur. Phys. J. E **18**, 287 (2005).
[17] P. M. Reis, R. A. Ingale, and M. D. Shattuck, Phys. Rev. Lett. **98**, 188301 (2007).
[18] C. Tapia-Ignacio, J. Garcia-Serrano, and F. Donado, Phys. Rev. E **94**, 062902 (2016).
[19] R. P. Ojha, P. A. Lemieux, P. K. Dixon, A. J. Liu, and D. J. Durian, Nature (London) **427**, 521 (2004).
[20] W. Wen, F. Kun, K. F. Pál, D. W. Zheng, and K. N. Tu, Phys. Rev. E **59**, R4758 (1999).
[21] P. G. de Gennes and P. A. Pincus, Phys. Kondens. Materie. **11**, 189 (1970).
[22] I. F. Sbalzarini and P. Koumoutsakos, J. Struct. Biol. **151**, 182 (2005).
[23] S. A. Schneider, W. S. Rasband, and K. W. Eliceiri, Nature Methods **9**, 671 (2012).
[24] P. Domínguez-García, S. Melle, J. M. Pastor, and M. A. Rubio, Phys. Rev. E **76**, 051403 (2007).
[25] P. Domínguez-García, J. M. Pastor, and M. A. Rubio, Eur. Phys. J. E **34**, 1 (2011).
[26] F. Donado, U. Sandoval, and J. L. Carrillo, Phys. Rev. E **79**, 011406 (2009).
[27] J. W. Swan, J. L. Bauer, Y. Liu, and E. M. Furst, Soft Matter **10**, 1102 (2014).
[28] A. Milchev, Y. Rouault, and D. P. Landau, Phys. Rev. E **56**, 1946 (1997).
[29] Y. Rouault and A. Milchev, Phys. Rev. E **55**, 2020 (1997).
[30] R. Agustín-Serrano, F. Donado, and E. Rubio-Rosas, J. Magn. Mag. Mater. **335**, 149 (2013).

[31] M. A. Osipov, P. I. C. Teixeira, and M. M. Telo da Gama, Phys. Rev. E **54**, 2597 (1996).
[32] J. M. Tavares, J. J. Weis, and M. M. Telo da Gama, Phys. Rev. E **59**, 4388 (1999).
[33] P. C. Jordan, Mol. Phys. **38**, 769 (1979).
[34] A. Satoh and S. Kamiyama, J. Colloid Interface Sci. **172**, 37 (1995).
[35] B. J. de Gans, N. J. Duin, D. van den Ende, and J. Mellema, J. Chem. Phys. **113**, 2032 (2000).
[36] J. Huang and P. Lai, Physica A **281**, 105 (2000).
[37] F. Donado, J. L. Carrillo, and M. E. Mendoza, J. Magn. Mag. Mater. **320**, e354 (2008).
[38] P. I. C. Teixeira, J. M. Tavares, and M. M. Telo da Gama, J. Phys.: Condens. Matter **12**, R411 (2000).